

Phase field simulation of liquid phase separation with fluid flow

G. Tegze*, T. Pusztai, L. Gránásy

Research Institute for Solid State Physics and Optics, H-1525 Budapest,
POB 49, Hungary

Abstract

A phase-field theory of binary liquid phase separation coupled to fluid flow is presented. The respective Cahn–Hilliard-type and Navier–Stokes equations are solved numerically. We incorporate composition and temperature dependent capillary forces. The free energies of the bulk liquid phases are taken from the regular solution model. In the simulations, we observe Marangoni motion, and direct and indirect hydrodynamic interactions between the droplets. We find that coagulation is dramatically accelerated by flow effects. Possible extension of the model to solidification is discussed.

© 2005 Elsevier B.V. All rights reserved.

Keywords: Phase separation; Fluid flow; Coagulation; Marangoni motion; Phase-field theory

1. Introduction

Liquid phase separation plays a central role in a variety of production technologies. Phase separation in metastable liquids and in glasses is known to assist the nucleation of the crystalline phase [1]. Two-phase alloys produced by solidifying phase separating monotectic liquids are extensively used as self-lubricating bearing materials in automotive industry [2]. Efforts have been made to prepare structured monotectic textures via carefully controlling solidification [3]. The quality of the final products is determined by the microstructure of this type of alloys, which, in turn, is largely determined by complex phenomena taking place when the homogeneous liquid existing above the bimodal line is cooled through the two-phase region (see e.g., [1–4]). A variety of phenomena have been identified that influence the droplet dispersion in the phase separation stage:

1.1. Diffusion-related processes

- (i) Coagulation due to Brownian motion of the droplets (Binder–Stauffer (BS) mechanism) [5].
- (ii) Evaporation–condensation type interaction (Lifshitz–Slyozov–Wagner (LSW) mechanism) [6,7].

- (iii) Diffusion coupling, where the iso-concentration lines include two or more droplets, which then attract or repulse each other depending on the composition gradient (Tanaka’s first (T1) mechanism) [8].

1.2. Hydrodynamic effects

- (iv) Flow-assisted coagulation (FA).
- (v) Collision-induced collision, where the flow field of two coagulating droplets induces further coagulation events (Tanaka’s second (T2) mechanism) [9].
- (vi) Hydrodynamic coarsening driven by capillary instability (Siggia’s (S) mechanism) relevant for bicontinuous phase separation [10].

1.3. Hydrodynamic effects coupled to external fields

- (vii) Marangoni motion (M): Thermo-capillary forces drive the droplets with a velocity increasing with size, thus large droplets capture smaller droplets.
- (viii) Stokes motion (St): Buoyancy forces drive the droplets with a velocity increasing with the square of the linear size, thus large droplets capture smaller droplets.

Herein, we present a phase-field theory of liquid phase separation in the presence of viscous flow that incorporates most of these mechanisms. In this work, we concentrate exclusively on liquid phase separation in the absence of gravity. We compute

* Corresponding author. Tel.: +36 1 392 2222x3155; fax: +36 1 392 2219.
E-mail address: turpi@szfki.hu (G. Tegze).

the time evolution of the size distribution of droplets and discuss the roles the individual processes may play in shaping the droplet distribution.

2. Phase-field theory of liquid phase separation with fluid flow

In our approach, the local state of the matter is characterized by the chemical composition, c . The free energy F consists of two contributions discussed below:

$$F = \int d^3r \left\{ \frac{\varepsilon_c^2}{2} |\nabla c|^2 + f_L(c, T) \right\}, \quad (1)$$

where ε_c is a constant, T is the temperature. The gradient term for c leads to a diffuse liquid–liquid interface, a feature observed both in experiment and computer simulations. The local free energy density $f_L(c, T)$ provides the driving force for phase separation. It has been taken here from the regular solution model, $f_L(c, T) = (1 - c)f_A^L + cf_B^L + [\Omega_L + T d\Omega_L/dT]c(1 - c)/v_m + RT\{c \ln c + (1 - c) \ln(1 - c)\}/v_m$, where v_m is the molar volume and R the gas constant. For the sake of simplicity, we assume that the molar volume of the two constituents is the same.

Time evolution is governed by relaxational dynamics, and a Langevin noise term (random flux ζ_j) is added to model thermal fluctuations (essentially a Langevin equation based on the time dependent Ginzburg–Landau formalism [11]). The usual equation of motion for c is supplemented here with the appropriate convection term

$$\frac{\partial c}{\partial t} + (\vec{v} \cdot \nabla)c = \nabla \cdot \left\{ M_c \nabla \left[\left(\frac{\partial f}{\partial c} \right) - \nabla \cdot \left(\frac{\partial f}{\partial \nabla c} \right) - \zeta_j \right] \right\}. \quad (2)$$

The time scale of phase separation is determined by the coarse-grained mobility $M_c = (v_m/RT)Dc(1 - c)$ [12], where D is the diffusion coefficient.

Coupling to the melt flow has been done as described by Conti [13–15]. We assume here an incompressible, viscous liquid, and that the mass density is independent of composition and phase. The mass and momentum balance are described by the equations

$$\frac{\partial \rho}{\partial t} + \rho \nabla \cdot \vec{v} = 0, \quad (3)$$

and

$$\rho \frac{\partial \vec{v}}{\partial t} + \rho(\vec{v} \cdot \nabla)\vec{v} = \rho \vec{g} + \nabla \cdot \mathbf{P}, \quad (4)$$

respectively. Here ρ is the mass density, \vec{v} the velocity, and \vec{g} is the gravitational acceleration, while

$$\mathbf{P} = \mathbf{I}[-p + \frac{1}{2}\varepsilon_c^2 T(\nabla c)^2] - \varepsilon_c^2 T(\nabla c \otimes \nabla c) + \mathbf{\Pi} \quad (5)$$

is the non-classical stress tensor [13–15]. The latter is divided into a non-dissipative part (that includes the capillary terms emerging from spatial variation of the concentration field) and into a dissipative part represented by the viscous stress tensor $\mathbf{\Pi}$. (\mathbf{I} is the unit tensor, while \otimes stands for diadic product.)

Note that for small deviations from the average concentration, the equation of motion for the concentration field boils down to the Cahn–Hilliard equation.

3. Numerical solution and evaluation of results

The equation of motion (Eq. (2)) have been solved numerically on an equidistant rectangular grid using an explicit finite difference scheme. In contrast, the hydrodynamic equations (Eqs. (3)–(5)) have been solved on a respective staggered grid by an explicit finite volume method. Rectangular grids of sizes 200×200 , 250×250 , 500×500 , and 1000×1000 were used. We applied periodic boundary conditions except the Marangoni study, where to avoid a continuous acceleration of the drop due to the finite simulation window, we assumed no-flux boundary conditions.

The noise has been discretized as described by Karma and Rappel [16]. A parallel code has been developed and run on two PC clusters, consisting of 60 and 100 nodes, respectively.

The size distribution of the droplets has been evaluated from the chemical composition maps using the software ImageJ.

4. Physical properties

The computations were performed with the physical properties of the Al–Bi system. The free energies have been obtained from the regular solution model, whose parameters were chosen so that the corresponding phase diagram (Fig. 1) reflects the main features of the experimental one. The melting point, the heat of fusion and the (average) molar volume of the pure constituents were taken as $T_A = 933.3$ K, $H_{f,A} = 10.79$ kJ/mol, $T_B = 544.5$ K, $L_A = H_{f,A} = 11.3$ kJ/mol, $v_m = 15.7$ cm³/mol, while the interaction parameter and its temperature coefficient were assumed to be $\Omega_S = 42$ kJ/mol and $d\Omega_S/dT = -10$ J/mol/K in the solid and $\Omega_L = 32$ kJ/mol and $d\Omega_L/dT = -10$ J/mol/K in the liquid, respectively.

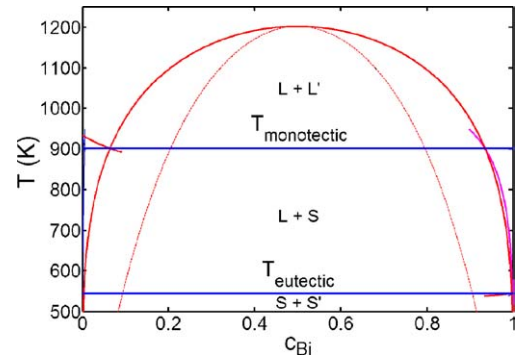


Fig. 1. Phase diagram of the Al–Bi system calculated using the regular solution model. The liquid compositions for the two-phase equilibria (liquidus and liquid bimodal lines and their metastable continuations) are denoted by red lines, while the red dotted line stands for the liquid spinodal. The temperatures for three-phase equilibria (monotectic and eutectic temperatures) are denoted by blue horizontal lines.

The interfacial free energy at the monotectic temperature is taken $\gamma = 60 \text{ mJ/m}^2$ [17]. To enhance the thermo-capillary effects, we increased $d\gamma/dT$ by a factor of ~ 30 .

In the calculations, we fix the temperature to $T = 902 \text{ K}$ and the initial chemical composition $c_0 = 0.25$. This exceeds slightly the monotectic temperature, therefore no solidification occurs, and falls inside the spinodal region. Thus the time scale of the processes is set by the interplay of melt flow and chemical diffusion. Accordingly, the equation of motion has been made dimensionless using the length and time scales of $\xi = 6 \times 10^{-6} \text{ cm}$, $\tau = \xi^2/D = 1.2 \text{ }\mu\text{s}$, where $D = 3 \times 10^{-5} \text{ cm}^2/\text{s}$. The dimensionless time and spatial steps were chosen as $\Delta t = 1.25 \times 10^{-7}$ and $\Delta x = 5 \times 10^{-3}$. The upper limits of the time period and the linear size of our simulations fall in the μs and μm range, respectively.

The viscosity has been taken to be 1 mPa s .

5. Results and discussion

First we illustrate that our model includes all the mechanisms mentioned in the introduction with the exception of the Brown motion (BS) and the gravity driven (St) coagulation of the droplets. Work is underway to incorporate these mechanisms.

5.1. Diffusion controlled processes (LSW, T1)

In the *diffusion-based* LSW mechanism for asymmetric droplets, the larger droplet grows on the expense of the smaller one (Fig. 2(a)). In the case of symmetric droplets without melt flow, the *diffusion-controlled* T1 mechanism applies. Depending on the concentration gradient they either coagulate (Fig. 2(b)) or move away from each other.

5.2. Hydrodynamic effects (FA, T2, S)

The effect of melt flow on two coagulating droplets is illustrated in Fig. 2(b) and (c). In the absence of flow, the rate-limiting factor is chemical diffusion, and coagulation happens on the diffusive time scale. The presence of melt flow dramatically accelerates the merging the two droplets (Fig. 2(c)). The final

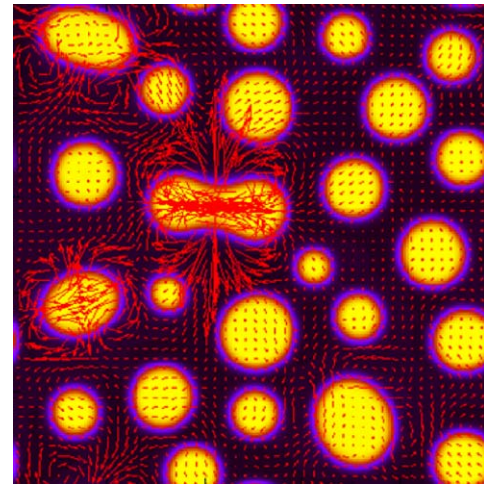


Fig. 3. “Collision-induced collision” in phase separating Al–Bi system. Note the flow field that induces a chain of coagulation events. Coloring is the same as for Fig. 2. (Computed on a 200×200 grid.)

droplet formed by coagulation performs oscillations that are damped in time by viscous dissipation. This flow assisted (FA) coagulation of droplets is orders of magnitude faster than the purely diffusive T1 mechanism (cf. Fig. 2(b) and (c)). These findings are in accord with results on transparent liquids [9].

Complex hydrodynamic interactions occur in the presence of large number of droplets. As pointed out by Tanaka [10], the flow field generated by two collapsing droplets shown in Fig. 2(b) moves closer the droplets at the far ends of the collapsing droplets, while it pushes them farther on the elongated sides. When the inter-droplet distance is small, these motions often induce further coagulation events (mechanism T2). We observe such chains of coagulation events in our simulations (see e.g., Fig. 3).

In the bicontinuous phase separation studies, performed close to the critical composition, where the two liquid phases develop in comparable volume, we observe rupturing of the interface due to capillary instabilities (Fig. 4) and “double phase separation”, phenomena reported by several authors [18–20].

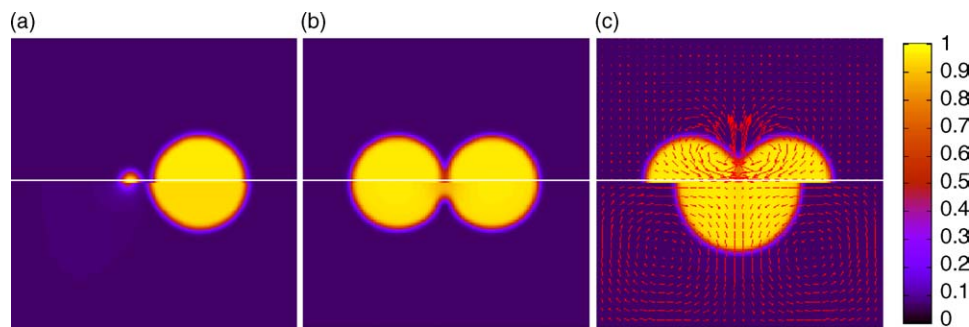


Fig. 2. Coarsening mechanisms for two droplets as predicted by the phase-field theory. (a) Lifshitz–Slyozov–Wagner (LSW) mechanism. Upper and lower parts are from snapshots taken at 1.25×10^{-4} and 1.875×10^{-3} dimensionless times. (b) Diffusion controlled coagulation (T1). Upper and lower parts are from snapshots taken at 1.25×10^{-4} and 2.5×10^{-2} dimensionless times. (c) Flow assisted (FA) coagulation. Upper and lower parts are from snapshots taken at 1.25×10^{-4} and 9.375×10^{-4} dimensionless times. The red arrows indicate the velocity field. Composition maps are shown. The color bar shows the relation between Bi concentration and colors. Note the sluggishness of the purely diffusive processes (LSW and T1), the strong outward flow building up along the vertical axis between the two collapsing drops, and the weak inward flow along their horizontal axis. (Computed on a 200×200 grid.)

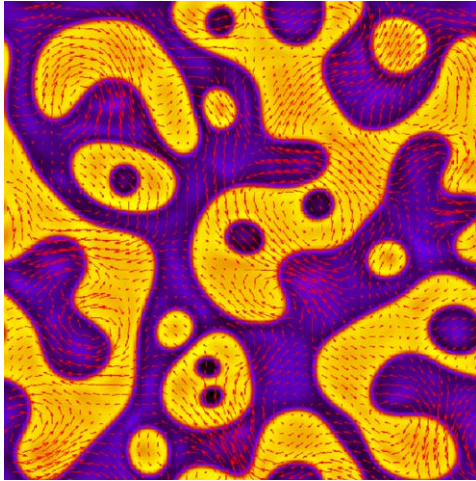


Fig. 4. Bicontinuous phase separation: capillary-instability-driven rupturing of the interface, and “double phase separation” at 50% Bi concentration. Coloring is the same as for Fig. 2. (Computed on a 500×500 grid.)

5.3. Hydrodynamic effect coupled to external fields: Marangoni motion (M)

The motion of Bi rich liquid droplets in an Al rich liquid has been studied in a constant temperature gradient. Fig. 5(a) and (b) display the flow fields developing inside the droplets in the laboratory frame and in a coordinate system fixed to the geometrical center of the droplet, respectively. In agreement with analytical predictions (for review see [21]), we find that the steady state velocity increases with increasing droplet diameter (Fig. 5(c)). We also observe, that the growth rate increases both with the temperature gradient, and with the temperature coefficient of the surface tension, as follows from analytical theory [21].

5.4. Size-distribution of droplets

Having demonstrated that the essential phenomena are incorporated into our phase field model, we investigate the effect of the hydrodynamic flow and thermo-capillary forces on the droplet size distribution on a grid of size 1000×1000 . We com-

pare three cases: (I) purely diffusive interaction; (II) diffusive and hydrodynamic interactions; (III) diffusive and hydrodynamic interactions in the presence of a temperature field that increases linearly towards the vertical centerline of the simulation window from both sides.

The late-stage morphologies of the three cases are compared in Fig. 6(a)–(c). The spatially homogeneous droplet microstructures observed in cases I and II are fairly similar (though formed on different time scales). In case III, there is an apparent accumulation of large droplets at the vertical centerline, while droplet-free zones evolve at the vertical sides of the simulation window, phenomena attributable to the Marangoni motion of droplets.

The time evolution of the respective droplet size distributions reveals more differences, as shown in Fig. 6(d)–(f). In case I, we observe a Lifshitz–Slyozov–Wagner type asymmetric droplet size distribution, with a long tail towards the small sizes (Fig. 6(a)). In case II, the presence of hydrodynamic effects accelerates droplet coarsening. At early stages a bimodal distribution with a sharp peak at small sizes appears. The amplitude of this peak reduces with time, and a broad, nearly symmetric size distribution develops. At later stages (not shown here), we observe several weak peaks, however, further work and better statistics are needed to assess their significance. In case III, formation of large droplets at the vertical centerline is assisted by Marangoni motion of droplets towards this position. (The larger droplets are faster, and thus can capture smaller droplets moving at a lower velocity.) While in the late stages of the phase transition, the width and shape of the droplet distribution are comparable to those observed in case II, here we do not observe a bimodal distribution at early times.

Finally, we mention that the present formulation of the phase-field theory of liquid phase separation is a suitable starting point for developing a model to address multi-particle solidification in phase separating liquids in the presence of fluid flow, as it is compatible with recent models of polycrystalline freezing [22–27]. Work is underway to incorporate two structural order parameters: the phase field that monitors the freezing and an orientational field that describes the local crystallographic orientation in the laboratory frame. Such an approach will enable us to model the nucleation, growth, and motion (including rotation) of anisotropic crystal particles in phase separating melts.

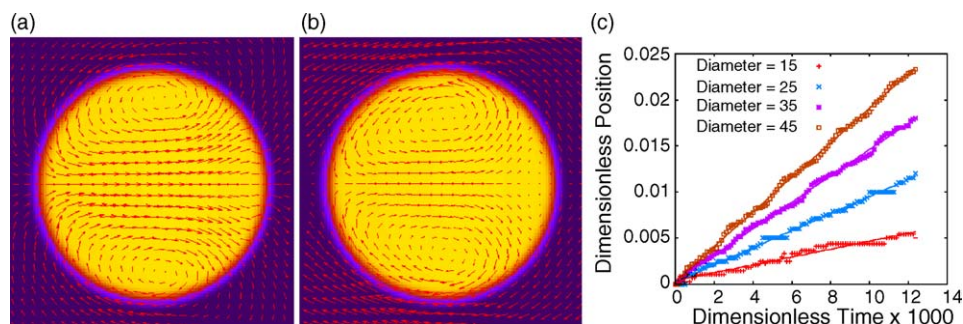


Fig. 5. Marangoni motion as predicted by the phase-field theory. Close-ups on the flow field and the concentration map of a 24 nm droplet are shown: (a) the velocity field in the laboratory frame, and (b) the velocity field in the coordinate system fixed to the geometrical center of the droplet, (c) droplet position is displayed as a function of time. Lines are to guide the eyes. Coloring of panels (a) and (b) is the same as for Fig. 2. The simulations were performed on a 250×250 grid. The temperature increases linearly from left to the right.

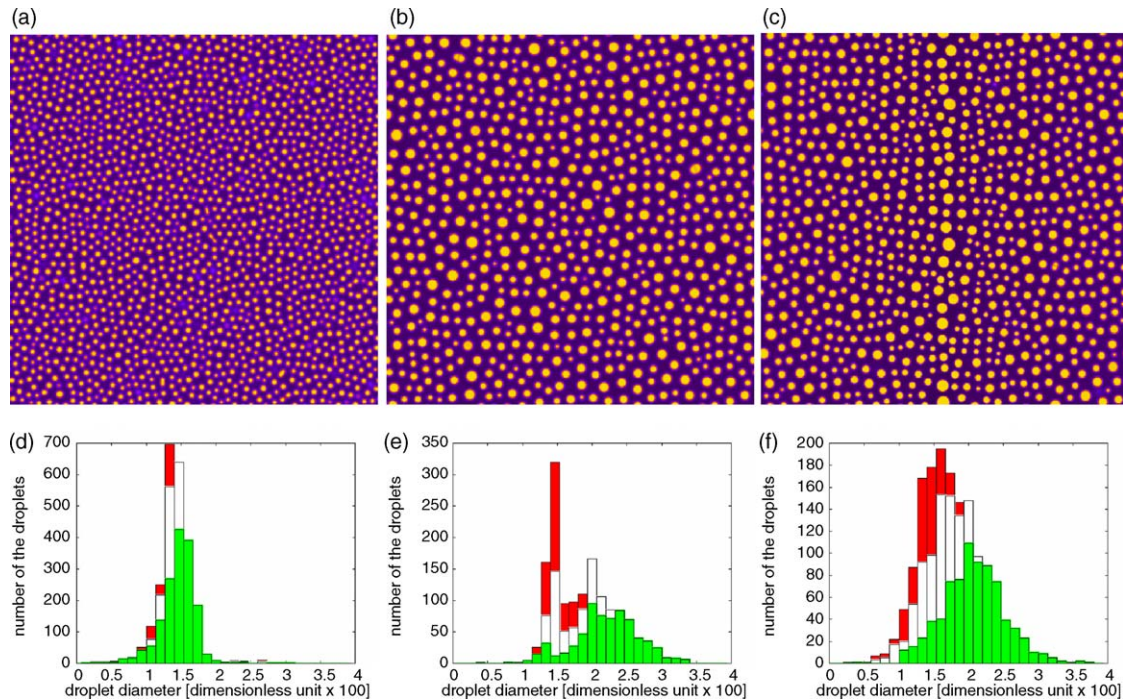


Fig. 6. Liquid phase separation in Al–Bi as predicted by the phase-field theory on a 1000×1000 grid. (a) Without melt flow, (b) with melt flow, (c) with melt flow and a temperature field that increases linearly towards the vertical centerline of the simulation. Snapshots of the concentration fields taken at dimensionless time 0.051 are shown. Coloring is the same as for Fig. 1. Histograms showing the respective droplet size distributions at three dimensionless times (0.025, 0.031, and 0.051 denoted by the red, white and green columns) for the three cases are presented in panels (d)–(f), respectively.

6. Summary

We presented a phase-field theory of liquid phase separation in monotectic alloys in the presence of melt flow. It has been shown that our model properly describes the various mechanisms contributing to the coarsening of the droplets. We have shown that besides dramatically accelerating coagulation, the hydrodynamic effects lead to the formation of a broader bi-/multi-modal droplet distribution, as opposed to the usual Lifshitz–Slyozov–Wagner type unimodal droplet distribution characteristic to purely diffusive processes. We found that Marangoni motion in a temperature field that increases linearly towards the centerline of the simulation window, and yields a broad, nearly symmetric droplet size distribution.

Acknowledgments

The authors thank M. Conti and M. Tegze for the enlightening discussions. This work has been supported by contracts OTKA-T-037323 and ESA PECS No. 98021, and forms part of the ESA MAP Project No. AO-99-026 “MONOPHAS”. T.P. acknowledges support by the Bolyai János Scholarship of the Hungarian Academy of Sciences.

References

- [1] A.H. Ramsden, P.F. James, *J. Mater. Sci.* 19 (1984) 1406.
- [2] L. Ratke, S. Dieffenbach, *Mater. Sci. Eng.* R15 (1995) 263.
- [3] H. Yasuda, I. Ohnaka, S. Fujimoto, A. Sugiyama, Y. Hatashi, M. Yamamoto, A. Tsichiyama, T. Nakano, J. Uesugi, K. Kishio, *Mater. Lett.* 58 (2004) 911.
- [4] J. Fan, S. Ji, J. Zhang, *Mater. Sci. Technol.* 17 (2001) 873.
- [5] K. Binder, D. Stauffer, *Adv. Phys.* 25 (1976) 343.
- [6] L.M. Lifshitz, V.V. Slyozov, *J. Phys. Chem. Solids* 19 (1961) 35.
- [7] C. Wagner, *Z. Electrochem.* 65 (1961) 581.
- [8] H. Tanaka, *J. Chem. Phys.* 103 (1995) 2361.
- [9] H. Tanaka, *J. Chem. Phys.* 105 (1996) 10099.
- [10] E.D. Siggia, *Phys. Rev. A* 20 (1979) 595.
- [11] J.P. Gunton, M.S. Miguel, P.S. Sahni, in: C. Domb, J.L. Lebowitz (Eds.), *Phase Transitions and Critical Phenomena*, vol. 8, Academic, NY, 1983, p. 267.
- [12] J.A. Warren, W.J. Boettinger, *Acta Met. Mater.* 43 (1995) 689.
- [13] M. Conti, *Phys. Rev. E* 64 (2001) 051601.
- [14] M. Conti, M. Fermani, *Phys. Rev. E* 67 (2003) 026117.
- [15] M. Conti, *Phys. Rev. E* 69 (2004) 022601.
- [16] A. Karma, W.-J. Rappel, *Phys. Rev. E* 60 (1999) 3614.
- [17] W. Hoyer, I. Kaban, M. Merkwitz, *J. Optoelectr. Adv. Meter.* 5 (2003) 1069.
- [18] P. Wiltzius, A. Cumming, *Phys. Rev. Lett.* 66 (1991) 3000.
- [19] H. Tanaka, *Phys. Rev. E* 51 (1995) 1313.
- [20] H. Tanaka, T. Araki, *Phys. Rev. Lett.* 81 (1998) 389.
- [21] L. Ratke, W. Thieringer, *Acta Metall.* 33 (1985) 1793.
- [22] R. Kobayashi, J.A. Warren, W.C. Carter, *Physica D* 119 (1998) 415.
- [23] L. Gránásy, T. Börzsönyi, T. Pusztai, *Phys. Rev. Lett.* 88 (2002) 206105.
- [24] J.A. Warren, R. Kobayashi, A.E. Lobkovsky, W.C. Carter, *Acta Mater.* 51 (2003) 6035.
- [25] L. Gránásy, T. Pusztai, J.A. Warren, T. Börzsönyi, J.F. Douglas, V. Ferreira, *Nat. Mater.* 2 (2003) 92.
- [26] L. Gránásy, T. Pusztai, T. Börzsönyi, J.A. Warren, J.F. Douglas, *Nat. Mater.* 3 (2004) 635.
- [27] L. Gránásy, T. Pusztai, J.A. Warren, *J. Phys. Condens. Matter* 16 (2004) R1205.